A Coupled Rotor/Wing Optimization Procedure for High Speed Tilt-Rotor Aircraft

Thomas R. McCarthy
Graduate Research Assistant

Aditi Chattopadhyay
Associate Professor

Department of Mechanical and Aerospace Engineering
Arizona State University
Tempe, Arizona

A multidisciplinary optimization procedure is developed to investigate the design trade-offs associated with coupled rotor/wing performance in high speed tilt-rotor aircraft. The aerodynamic efficiency of the rotor in both hover and high speed cruise are improved along with the aerodynamic and aeroelastic performance of the wing while maintaining structural integrity of the wing/rotor configuration. The objectives are to maximize the hover figure of merit and the high speed cruise propulsive efficiency of the rotor and to minimize the wing weight. Constraints on the rotor include the first natural frequency in hover, the autorotational inertia and the blade weight. To avoid whirl flutter instabilities, constraints are imposed on the real part of the stability roots in the windmill flight condition. Constraints are also imposed on wing root stresses in both hover and cruise. An isotropic box beam model is used to represent the structural properties of the wing-box section. Design variables include rotor and wing planform variables and individual wall thicknesses in the wing. The Kreisselmeier-Steinhauser function approach is used to formulate the multiobjective optimization problem and the Broyden-Fletcher-Goldfarb-Shanno method is used as the optimization algorithm. The two-point exponential expansion approximation technique and a variable move limit scheme are used to reduce the computational effort. The optimum design performance is compared with an existing advanced tilt-rotor performance which is used as the baseline design. The results show significant improvements in both aerodynamic and structural performance while maintaining aeroelastic stability.

Nomenclature

A	Cross-sectional area of the wing box beam, ft^2
AI	Autorotational inertia, $lb\text{-}ft^2$
b	Wing span, ft.
C	Wing chord, ft
c	Blade chord, ft.
$c_{l\alpha}$	Lift curve slope
c_o-c_3	Blade chord distribution parameters
C_P	Coefficient of power
C_r	Wing root chord, ft.
C_T	Coefficient of thrust
C_t	Wing tip chord, ft.
EI_{xx}	Lagging stiffness, $lb\text{-}ft^2$
EI_{zz}	Flapping stiffness, $lb\text{-}ft^2$
f_1	First natural frequency in hover, per rev
F_k	Vector of original objective functions
f_k	K-S function constraint vector
F_{KS}	K-S objective function
FM	Hover figure of merit
FS	Factor of safety
$F_{\tilde{k}}$	Vector of reduced objective functions
GJ	Torsional rigidity, $lb\text{-}ft^2$
g_j	Original constraint vector
I_θ	Polar moment of inertia, $slug\text{-}ft^2$
k_r	Nondimensional blade radius of gyration
L	Wing lift, lb
m	Blade sectional mass, slug/ft
NCON	Number of original constraints
NMODE	Total number of flutter modes considered in cruise
NOBJ	Number of objective functions
NSEG	Number of wing segments
P	Rotor power, hp
p_n	Two-point exponential expansion exponent
T	Rotor thrust, lb
t_{io}-t_{i3}	Wall thickness distribution parameters, ft
V_∞	Free stream velocity, ft/s^2
W_{blade}	Rotor blade weight, lb
W_{total}	Combined wing/rotor weight, lb
W_{wing}	Wing weight, lb
$\dot{w}$	Wing flapping velocity, ft/s
X_a	Wing elastic axis offset, ft
x_{ac}	Blade lifting line offset, ft.
$\bar{y}$	Nondimensional radial location, y/R
α_b	Blade angle of attack, deg.
α_w	Wing angle of attack, rad.
δ	K-S function draw down factor
Φ	Design variable vector
η_c	Propulsive efficiency
λ	Taper ratio
Λ_k	Real part of the kth stability root
θ	Blade twist, deg.

Presented at 51st Annual Forum of AHS, Ft. Worth, TX, May 8-11, 1995. Manuscript submitted October 1995; approved July 1996.

θ_1-θ_3 Blade twist distribution parameters
ρ Density of the beam, slug/ft^3
ρ_∞ Air density, slug/ft^3
σ Area-weighted solidity of the rotor
σ_{al} Allowable stress, p.s.i.
τ_{oct} Octahedral wing stress, p.s.i.
υ Minimum allowable blade damping
ζ Nondimensional wing span, y/b

Subscripts
c cruise
h hover
max maximum value
ref reference, or baseline, values

Introduction

The concept of high speed vertical take-off and landing (VTOL) aircraft has been of interest over the past few decades of rotorcraft development. Over the past several years, a number of concepts have been presented to meet these goals. Of these, the tilt-rotor aircraft has emerged as a viable concept. The primary design objectives of the high speed civil proprotor are improved cruise propulsive efficiency and acceptable hover performance. The design guidelines also include cruise speeds in the range of 350 to 500 knots. This introduces the problem of aeroelastic stability which generally dictate the stiffness requirements of the wing structure. During cruise, when the aircraft is flying in the airplane mode, the wing is the primary source of lift. Also, while in hover the download effect of the rotor on the wing is on the order of 12 percent of the total rotor thrust (Ref. 1). Therefore, the aerodynamic performance and the structural and aerodynamic loading on the wing become important design issues.

At a high enough forward speed, the tilt-rotor aircraft experiences whirl flutter instability which arises due to the coupled flexible motions of the wing, the pylon and the rotor. The principal cause for such instability is the destabilizing aerodynamic forces generated by the motion of the rotor on its support structure. Since civil tilt-rotors must be designed to be stable to a 20% margin above their dive speed, this means that the flutter speed must be about 650 knots for a cruise speed of 450 knots. The above problem becomes more complicated with the conflicting design issues associated with the rotor design. For example, lower wing thickness ratios, as required for improving compressibility drag, is generally detrimental to aeroelastic stability. Therefore, a rotor designed with thin airfoils for high speed cruise and high solidity for hover further contributes to the reduced stability of the high speed proprotor. Also, the forward sweep design of the wing further deteriorates the stability through increased torsional participation in the wing bending modes as does the mass offset of rotor pylon mounted at the wing tip. Therefore, to address the whirl flutter problem in cruise, the wing needs to be analyzed and proper stiffness and elastic coupling must be determined for proper frequency placement to minimize wing chordwise motions at the rotor hub.

Recently, research efforts have been initiated by Chattopadhyay et al. (Refs. 2-8) to develop formal optimization techniques to address the conflicting issues involving tilt-rotor design. In Refs. 2 and 3 optimization procedures were developed to maximize the high speed cruise propulsive efficiency without degrading the hover figure of merit. The problem of individual blade aeroelastic stability in high speed cruise was included in the optimization formulation in Ref. 4. In Ref. 5, the drive system weight was minimized and the associated trade-off in cruise efficiency was investigated. The integrated aerodynamic, aeroelastic and structural optimization of the rotor was addressed in Ref. 6. In Ref. 7, a purely aerodynamic multiobjective optimization procedure was reported for improved high speed cruise and hovering performance using planform and airfoil characteristics as design variables. In Ref. 8, the aerodynamic and structural design criteria in both high speed cruise and hover were addressed by developing a multilevel decomposition based optimization procedure. In all of the above work, the rotor design was the primary concern and only the rotor planform parameters and geometric properties were included as design variables in the optimization formulation.

The influence of the wing, however, is a critical design issue and requires an in-depth study. Therefore, the development of a multidisciplinary optimization procedure involving simultaneous rotor-wing design can be a very useful tool to help understand the various instabilities which ultimately affect the aircraft design. This paper represents the results of a recent research effort aimed at studying the various trade-offs associated with such a design. In this paper, the designs of the rotor and the wing are simultaneously addressed using a formal multiobjective optimization technique.

Rotor/Wing Geometric Modeling

The reference aircraft is a mathematical representation of the XV-15 tilting proprotor aircraft. The rotor is a three-bladed, gimballed rotor with a 25 foot diameter. These rotors are mounted at the tips of each of the wings. The wing has a rectangular planform with a span of 35.17 feet and an aspect ratio of 7.32. The load carrying member of the wing structure is modeled as a cantilever box beam with a rectangular cross section. For this simplified model to be representative of the realistic XV-15 wing design, the initial wall thicknesses along the wing span are determined using a simple optimization technique such that bending and torsional stiffness distribution of the box beam model are representative of original XV-15 design. Further, the first three frequencies, the generalized masses and the mode shapes at the rotor pylon are also designed to match NASTRAN data of the detailed XV-15 structural model (Refs. 9,10). The following sections describe the geometric modeling of the planform and cross sections of the rotor and the wing.

Rotor Model

The rotor planform characteristics are defined as follows. The chord, $c(\bar{y})$, and twist angle of attack, $\theta(\bar{y})$, are defined to have the following cubic spanwise distributions.

$$\theta(\bar{y}) = \theta_1(\bar{y} - 0.75) + \theta_2(4(\bar{y} - 0.75)^2 - 3\,(\bar{y} - 0.75)) + \theta_3(15(\bar{y} - 0.75)^3 - 20(\bar{y} - 0.75)^2 + 6(\bar{y} - 0.75)) \quad (1)$$

$$c(\bar{y}) = c_0 + c_1\bar{y} + c_2(4\bar{y}^2 - 3\bar{y} + c_3(15\bar{y}^3 - 20\bar{y}^2 + 6\bar{y}) \quad (2)$$

The offset in the twist distribution $(\bar{y} - 0.75)$ is used to ensure zero twist at 75 percent span. The shape functions used in these distributions are selected to maintain orthogonality between the functions over the range 0 to 1 which is beneficial to the optimization algorithm. These cubic distributions are selected to give the optimizer sufficient flexibility since the parameters which define these distributions are used as design variables.

A perturbational model, based on the chord distribution, is used to calculate the structural properties. This model is used to simplify the problem which in turn reduces the complexity of the design space. In this model, the blade stiffness properties are assumed to vary, from the reference values (Ref. 8), as follows.

$$\frac{EI_{xx}}{EI_{xx_{ref}}} = \left(\frac{c(\bar{y})}{c_{ref}(\bar{y})}\right)^4 \quad (3)$$

where EI_{xx} is the flapping stiffness and $c(\bar{y})$ is the chord. The lagging stiffness (EI_{zz}), the torsional rigidity (GJ) and the polar moment of inertia (I_θ) are defined similarly. The fourth order relation is used since, in general, these quantities are based on fourth order dependence of the beam width and height. Assuming that these quantities are directly proportional to the chord, the fourth order dependence on the chord is obtained. The blade sectional mass and radius of gyration distributions, $m(\bar{y})$ and $k_r(\bar{y})$, respectively, are assumed to be quadratic as follows.

$$\frac{m}{m_{ref}} = \left(\frac{c(\bar{y})}{c_{ref}(\bar{y})}\right)^2 \quad \text{and} \quad \frac{k_r}{k_{r_{ref}}} = \left(\frac{c(\bar{y})}{c_{ref}(\bar{y})}\right)^2 \tag{4}$$

The quadratic dependence is assumed for these quantities due to their dependence on the cross-sectional area, which in turn is assumed to be directly proportional to the chord. Similarly, the center of gravity, tension center and lifting line offsets from the elastic axis are assumed to vary linearly with the chord ratio. Although a detailed analysis is necessary for accurate representation of the blade structural response, this simplified analysis is useful in the preliminary design stage. The use of a complex finite element based procedure, within an optimization loop, can make the problem computationally prohibitive.

Wing Model

The aircraft wing is modeled as a cantilevered beam with tip masses representing the rotor system, transmission and engine pylon (Fig. 1). Although the reference wing planform is rectangular, the wing chord (C) is assumed to be linearly tapered to allow additional freedom to the optimizer as follows.

$$C = C_r[1 + \zeta(\lambda - 1)] \quad \text{where } \lambda = C_t/C_r \tag{5}$$

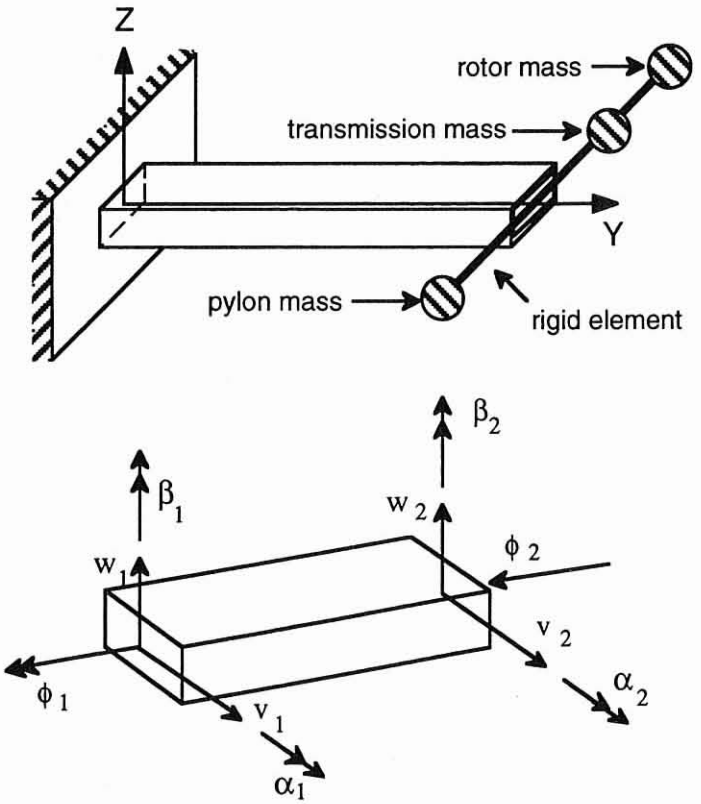

Fig. 1. Aircraft wing modeling.

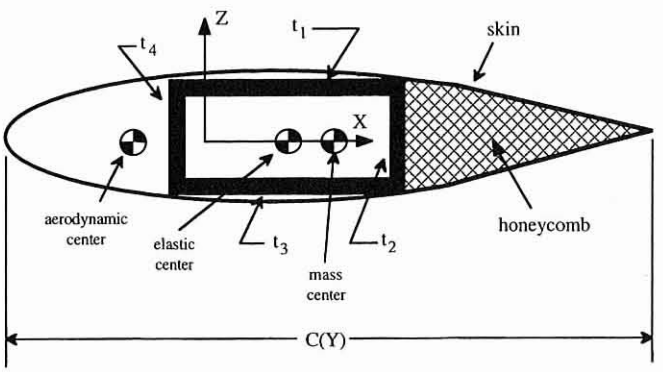

Fig. 2. Wing cross section.

The linear wing chord distribution is assumed to reduce the design space while still providing the optimizer the opportunity to change the wing planform since the root chord and taper ratio are used as design variables.

The load carrying structural member in the wing is modeled as a rectangular isotropic box beam with four independent wall thicknesses (Fig. 2). To reduce the number of design variables while keeping the design space sufficiently large, spanwise variations of wall thicknesses are assumed to be similar to the rotor chord and twist distributions as follows.

$$t_i(\zeta) = t_{i_0} + t_{i_1}\zeta + t_{i_2}(4\zeta^2 - 3\zeta) + t_{i_3}(15\zeta^3 - 20\zeta^2 + 6\zeta) \tag{6}$$

where the coefficients t_{i0} - t_{i3} describe the thickness distribution in each of the four walls (i=1,2,···, 4). Again, these cubic distributions are selected to provide the optimizer flexibility to alter these distributions as these parameters are all used as design variables.

Optimization Problem

The coupled rotor/wing optimization problem is performed simultaneously under three different flight conditions. The first flight condition corresponds to sea level hover and the second flight condition represents high speed cruise at an altitude of 25,000 feet. The third condition, which is used to investigate the aeroelastic stability of the coupled system, represents a high speed windmill condition at an altitude of 25,000 feet. This altitude is chosen because it is commonly used for tiltrotors operating in high speed cruise. The aeroelastic stability roots are calculated in a windmill condition as this is generally considered to be the most critical operating condition.

Objective Functions

The optimization problem addresses the simultaneous improvements in multiple design requirements. These are the maximization of the hover figure of merit (FM) and the propulsive efficiency in high speed cruise (η_c) and the minimization of the wing weight (W_{wing}). The hover figure of merit and the propulsive efficiency are defined as follows.

$$FM = \frac{P_{ideal}}{P} \tag{7a}$$

$$\eta_c = \frac{TV_\infty}{P} \tag{7b}$$

The wing weight is defined as follows.

$$W_{wing} = \int_0^b \rho A dx \tag{8}$$

Constraints

The following constraints are included in the optimization formulation to ensure efficient rotor and wing performance. To maintain rotor thrust at acceptable values during optimization, equality constraints are imposed on the thrust in hover and cruise. These constraints assume the following form.

$$T_h = T_{h_{ref}} \text{ and } T_c = T_{c_{ref}} \tag{9}$$

To avoid ground resonance, the first natural frequency in hover (f_1), which is a gimbal mode, is constrained to be above 1.2/rev to ensure that this frequency is not near 1/rev. The authors acknowledge that a more realistic formulation would include frequency placement of the first several modes as these frequencies will affect both rotor loads and vibratory hub shears (Ref. 11). However, in this preliminary study, only a lower bound is imposed on the first natural frequency. The autorotational inertia is constrained to be no less than 90 percent of the reference value to ensure that the optimum rotor can sufficiently autorotate in the event of engine failure. Since the autorotational inertia (AI) of the reference rotor is large, the minimum value of 90 percent of the reference value is selected to allow the optimizer more flexibility during the optimization process. An upper bound is imposed on the blade weight (W_{blade}) so that any reduction in the wing weight, which is an objective function, is not offset by an increase in the blade weight. These constraints are stated as follows.

$$f_1 \geq 1.20/\text{rev} \tag{10}$$

$$AI \geq 0.9\, AI_{ref} \tag{11}$$

$$W_{blade} \leq W_{ref} \tag{12}$$

Since both the rotor and the wing designs are altered during optimization, it is important to impose aeroelastic stability constraints to prevent any destabilization of the rotor/wing in high speed cruise. The rotor is mounted at the tip of the wing, therefore, the first several airframe modes, which are important for whirl flutter, are dominated by wing motion. To impose a factor of safety on the stability, the whirl flutter calculations are performed at the maximum dive speed which is 20 percent above the cruise condition. Also the blade, is trimmed to the windmill condition. These constraints are expressed as follows.

$$\Lambda_k \leq -\upsilon \qquad k = 1, 2, \cdots, \text{NMODE} \tag{13}$$

The quantity υ denotes the minimum allowable blade damping and is defined to be equal to 0.01.

Finally, constraints are imposed on the octahedral stresses at the root section of the wing box beam to ensure that the maximum stresses are below the allowable limit when multiplied by a factor of safety. These constraints assume the following form.

$$\tau_{oct} \times \text{FS} \leq \sigma_{al} \tag{14}$$

These stresses are calculated in both hover and cruise although they are more critical in hover.

Design Variables

To study the trade-offs associated with the simultaneous design of the rotor and the wing, design variables pertaining to both the rotor and the wing are used during optimization. The design variables for the rotor include the coefficients which define the spanwise chord and twist distributions (c_0 - c_3 and θ_1 - θ_3, respectively). As mentioned before, the shape functions used to describe the twist and the chord distributions are chosen to ensure orthogonality of the functions. Similarly the parameters that define the individual wall thicknesses in the wing-box (e.g. t_{ij}, i = 1, 2,$\cdots$, 4; j = 0, 1,$\cdots$, 3) are used as design variables. The wing root chord (C_r) and taper ratio (λ) are also included as design variables. It must be noted that in order to ensure that the blade chord and wing thickness distributions are realistic (that is, positive throughout the span) it is necessary to further impose geometric constraints on these distributions. The minimum allowable nondimensional chord value (c/R) is constrained to be 0.02 and the minimum allowable wall thickness in the wing (t_i) is constrained to be 0.064 inches. Although, the minimum allowable chord values are far too small at the root, these constraints are never near critical values except at locations near the tip.

Analysis

This section briefly describes the analysis procedures which are coupled within the optimization loop. This is followed by a description of the optimization technique.

Rotor Analysis

The rotor analysis is performed using CAMRAD (Ref.12) which calculates the section loading from the airfoil two-dimensional aerodynamic characteristics. The procedure uses the lifting line or blade element approach and includes corrections for yawed and three-dimensional flow effects. A wind tunnel trim option is used and the rotor is trimmed to a specific C_T/σ value using the collective blade pitch. The value of C_T/σ is calculated based on the prescribed values of thrust required at each flight condition. For the flutter calculations, a wind tunnel trim analysis is also performed. However, since this case is meant to be representative of a windmilling rotor, the rotor is trimmed to zero power. The aeroelastic stability analysis is performed using the axisymmetric flow assumption. The blade is discretized into 51 structural elements and 24 aerodynamic elements. Six bending degrees of freedom, six torsional degrees of freedom and two gimbal degrees of freedom are used to model the rotor. The first six symmetric wing modes are also included in the whirl flutter calculations to yield a total of 40 flutter modes. To reduce the computational effort, uniform inflow is assumed in all cases. The blade response is calculated in CAMRAD using rotating free-vibration modes equivalent to a Galerkin analysis. The blade is trimmed at each optimization cycle so that an intermediate design, which is a feasible design, represents a trimmed configuration.

Wing Analysis

The load carrying member of the wing is modeled as a box beam with a rectangular cross section (Fig. 2). The wing dynamic analysis is performed using an in-house developed code based on finite element analysis. Ten degrees of freedom are used to represent each beam element (Fig. 1). To model the geometric offset between the rotor hub and the elastic axis of the wing box beam, rigid elements are included at the wing tip. The cross-sectional properties of every beam element are

calculated using thin wall theory. The natural frequencies, generalized masses and generalized mode shapes at the tip of the wing, which describe the dynamic properties of the airframe, are then used as input to CAMRAD.

In order to evaluate flutter, the non conservative damping effect of aerodynamic forces must be included in the aerodynamic analysis. A lifting line theory which is based on the quasi-steady aerodynamic assumption is used to model the damping contribution from the effective angle of attack, $\dot{w}/V_\infty$. The lift (L), which acts at the quarter chord at a distance X_a from elastic center, can then be expressed as follows.

$$L = \frac{1}{2}\rho_\infty V_\infty^2 C c_{l\alpha}\left[\alpha_w + \frac{w}{V_\infty}\right] \tag{15}$$

Although a true unsteady aerodynamic formulation would be necessary for an accurate representation of the aerodynamic loads, the quasi-steady aerodynamic formulation is adequate for this preliminary design trade-off study (Ref. 13). Furthermore, the quasi-steady assumption significantly reduces the computational effort required to calculate the aerodynamic damping effect. This is particularly important in this optimization where the geometry of the wing planform changes during optimization process thus requiring several evaluations of the aerodynamic damping.

Optimization

Traditional optimization solution techniques require that only a single objective function be minimized or maximized. In this study, multiple objective functions are chosen, therefore, a multiobjective function formulation technique is required. The technique used is the Kreisselmeier-Steinhauser (K-S) function (Ref. 14) which has been found to perform very well in rotary wing applications (Ref. 3,6-8,15). Since the objective functions and the constraints must be evaluated several times before convergence is achieved, calculation of these values using exact analyses at each iteration is computationally prohibitive. Therefore the objective functions and constraints are approximated using a two-point exponential hybrid approximation technique (Ref. 16). Details of these techniques are described next.

Multiobjective Function Formulation

The first step in formulating the objective function in the Kreisselmeier-Steinhauser (K-S) function approach involves transformation of the original objective functions into reduced objective functions. Where the individual objective functions are to be minimized, these reduced objective functions assume the following form.

$$F_k^*(\Phi) = \frac{F_k(\Phi)}{F_{k_o}} - 1.0 - g_{max} \le 0 \quad k = 1,\cdots, NOBJ_{min} \tag{16a}$$

When the individual objective functions are to be maximized, the reduced objective functions are as follows.

$$F_k^*(\Phi) = 1.0 - \frac{F_k(\Phi)}{F_{k_o}} - g_{max} \le 0 \quad k = 1,\cdots, NOBJ_{max} \tag{16a}$$

where F_{k_o} represents the value of the original objective function F_k calculated at the beginning of each iteration and Φ is the design variable vector. The quantity g_{max} is the value of the largest constraint corresponding to the original constraint vector, $g_j(\Phi)$ (j = 1, 2,$\cdots$, NCON), and is held constant during each iteration. These reduced objective functions are analogous to constraints, therefore a new constraint vector $f_m(\Phi)$ (m = 1, 2,$\cdots$, M where M = NCON + NOBJ) is introduced which includes the original constraints and the constraints introduced by the reduced objective functions (Eqns. 16). The design variable vector remains unchanged. The new objective function to be minimized is defined using the K-S function as follows.

$$F_{KS}(\Phi) = f_{max} + \frac{1}{\delta}\ln\sum_{m=1}^{M} e^{\delta(f_m(\Phi)-f_{max})} \tag{17}$$

where f_{max} is the largest constraint corresponding to the new constraint vector $f_m(\Phi)$ and in general is not equal to g_{max}. The objective function $F_{KS}(\Phi)$, which represents an envelope function and includes the original objective functions and constraints, can now be minimized using any unconstrained optimization technique. In this research the Broyden-Fletcher-Goldfarb-Shanno (BFGS) algorithm (Ref. 17), a quasi-Newton method which uses an approximate Hessian matrix to compute the search direction, is used. Additional details can be found in Refs.3, 6-8, 13.

Approximate Analysis

The two-point exponential approximation technique, which was found to perform well in nonlinear optimization problems (Refs. 4-7,8), is used for the approximation of the objective functions and the constraints. This technique derives its name from the fact that the exponent used in the expansion is based upon gradient information from the previous and the current design cycles. Details of this technique are found in Ref. 15.

For the approximation to be valid, it is necessary to impose bounds, or "move limits" on the design variables during the optimization so that the design point remains in the neighborhood of the original point. These move limits represent a percent change from the original design variable. The move limits in this study are calculated using a variable scheme developed by Thomas et al. (Ref. 18). This algorithm adjusts the values of the move limits based on changes in the maximum violated constraint and also by tracking the individual move limits to see whether they reach the same upper or lower limit over two consecutive evaluations.

Results

The reference configuration used is a representation of the XV-15 aircraft which has a three-bladed gimballed rotor mounted at the tips of each wing (Ref. 9,10). The aerodynamic optimization is performed at a cruise altitude of 25,000 feet and a forward velocity of 300 knots with a rotational speed of 421 RPM. A vehicle weight of 13,000 pounds and an aircraft lift-to-drag ratio (L/D) of 5.3 is assumed. Therefore, the thrust in cruise is constrained to be at 1226 pounds for the two engine aircraft. In hover, the aircraft is assumed to be operating at sea level conditions with a rotational speed of 570 RPM. A 12 percent download effect from the rotor/wing interaction is used so that the thrust in hover is constrained to be at 7280 pounds. The flutter calculations are performed at a speed 20 percent above the cruise speed to represent the maximum dive speed (360 knots) and an altitude of 25,000 feet with a rotational velocity of 421 RPM. The blade is trimmed to the windmill condition for the calculation of the flutter roots. The operating conditions are summarized in Table 1.

The optimization problem converged after 30 cycles. After the first 10 cycles, the global move limit on every design variable was reduced from 10 percent to 5 percent in order to reduce oscillations of the objective functions. The optimization problem was performed on a Sun SparcStation 10 and required 3.04 C.P.U hours to converge.

The results from the optimization are presented in Table 2 and Figs.

Table 1. Summary of Flight Conditions.

Vehicle weight	13,000 lb
Blade radius	12.5
Hover	
Altitude	Sea level
Thrust, T_h	7280 lb
Rotational speed	570 RPM
Cruise	
Altitude	25,000 ft
Thrust, T_c	1226 lb
Rotational speed	421 RPM
Forward speed, V_∞	300 knots
Flutter	
Altitude	25,000 ft
Power, C_p	0.0
Rotational speed	421 RPM
Forward speed, V_∞	360 knots

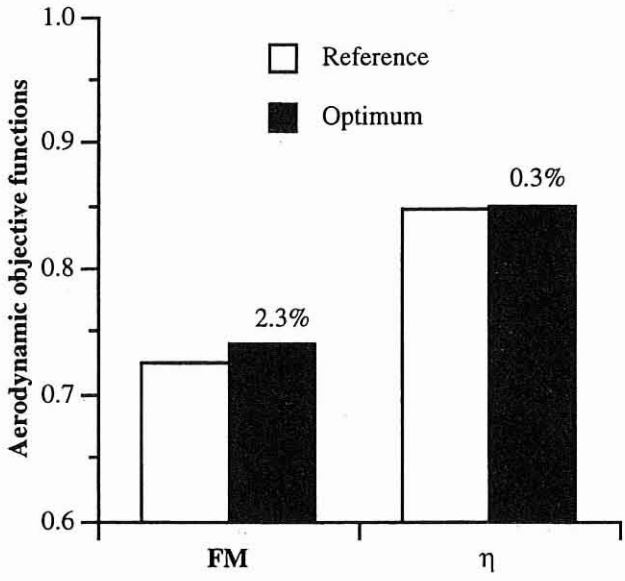

Fig. 3. Optimum aerodynamic results.

Table 2. Summary of Optimum Results.

	Bounds		Reference	Optimum
	Lower	Upper		
Objective functions				
FM			0.7246	0.7411
η_c			0.8475	0.8502
W_{wing}			704.3	606.1
Constraints				
f_1 (per rev)	1.200	-	1.291	1.327
AI (lb-ft^2)	3430	-	3811	3465
W_{blade} (lb)	-	213.4	213.4	200.0
W_{total} (lb)	-	-	1345	1206

3-14. From Table 2 and Fig. 3, it is seen that the aerodynamic objective functions are both improved. The hover figure of merit is increased by 2.3 percent while the propulsive efficiency in high speed cruise is slightly increased (0.3 percent) after optimization. A comparison of the weights is presented in Table 2 and Fig. 4 where it is seen that the wing weight (W_{wing}), which is also an objective function, is reduced by 14 percent from the reference value. The blade weight (W_{blade}) which is included only as a constraint is also reduced significantly (6.3 percent) from the reference value. Further, the total rotor/wing weight which is defined for the three bladed rotor as

$$W_{total} = W_{wing} + 3\,W_{blade} \tag{18}$$

is reduced by about 10 percent. These trends can be explained by examining the rotor and wing planforms.

The rotor blade chord distributions are presented in Fig. 5 and show that after optimization the blade chord has reduced values near the root and at the tip. This is due to the conflicting requirements posed by the hover and the cruise flight conditions. In hover, the rotor blade encounters negative angles of attack (α_b) at the tip which degrades performance (Fig. 6). The optimizer cannot simply reduce the twist at this location as this will degrade the high speed cruise propulsive efficiency. Similarly, the angle of attack distribution of the blade is negative near the root for the cruise condition (Fig. 7) and a simple increase in the twist at this location, to alleviate this problem, would degrade the hover figure of merit. The optimizer finds a compromise by slightly reducing the twist near the root (Fig. 8) which favorably alters the collective trim angle, but more importantly by increasing the chord over the midspan region of the blade which is beneficial to both flight conditions. The chord is then reduced near the root to improve the high speed cruise propulsive efficiency and is reduced at the tip to improve the hover figure of merit.

The wing chord distributions are presented in Fig. 9. It is seen from this figure that the root chord remains unchanged and a very small amount of taper is introduced ($\lambda = 0.99$). In order to closely match the first three natural frequencies and the generalized masses of the wing structure, the root stresses of the reference configuration become violated. Since only these stresses are critical, the optimizer allows slight

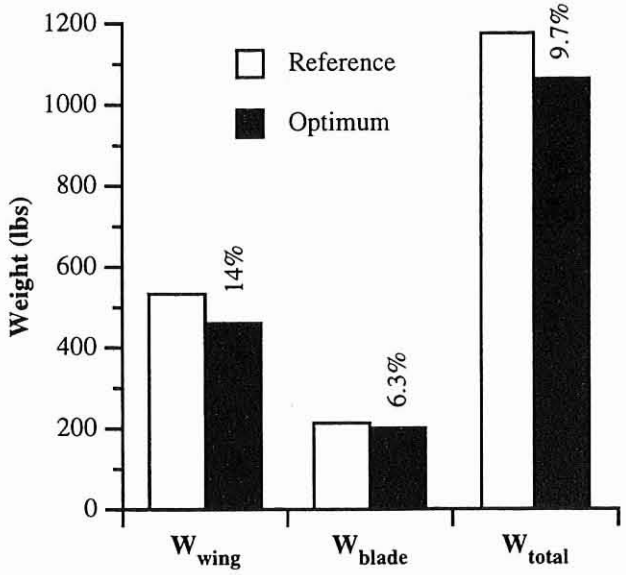

Fig. 4. Optimum structural results.

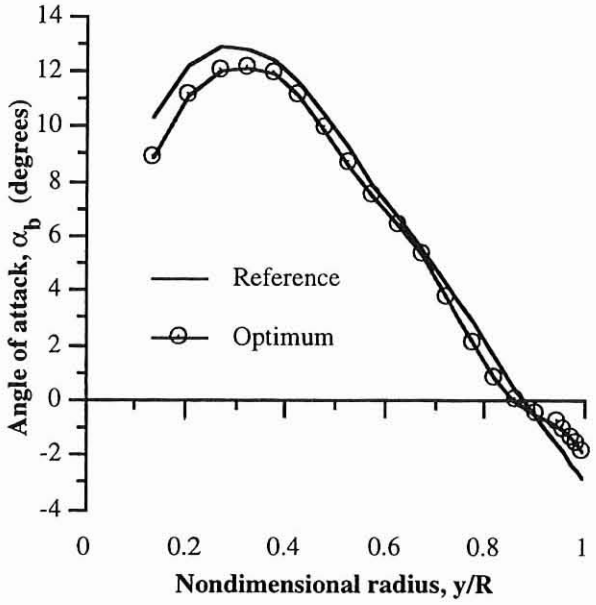

Fig. 6. Hover angle of attack distribution.

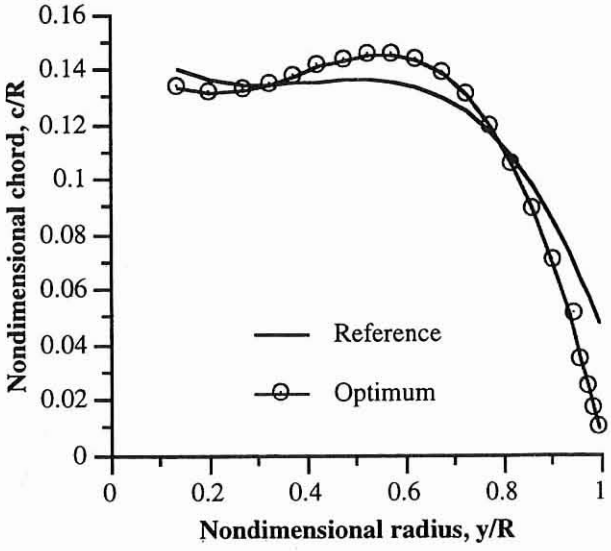

Fig. 5. Blade chord distributions.

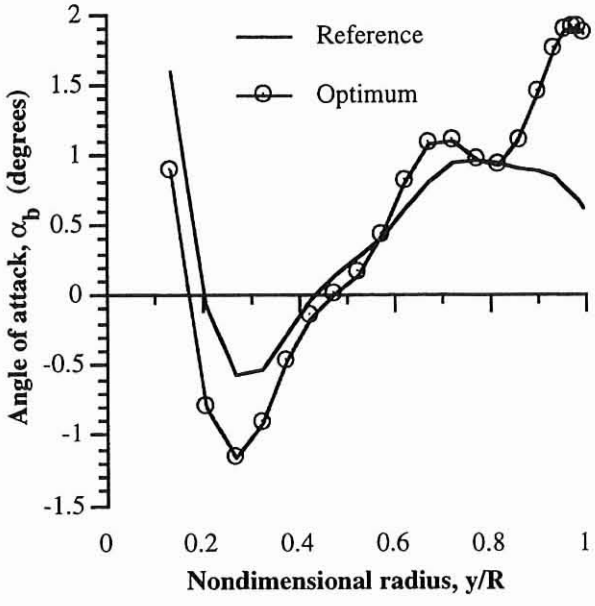

Fig. 7. High speed cruise angle of attack distribution.

taper in the wing chord distribution which in turn tapers the dimensions of the box beam without exceeding the allowable stresses. If too much taper is introduced to reduce the weight, the stiffness of the beam will be reduced at the tip of the wing. Due to the presence of the large tip mounted rotors, this can degrade the structural performance as well as the aeroelastic stability. Therefore, only a small taper is permissible in the wing chord distribution.

The horizontal wall thickness of the wing box beam are presented in Fig. 10a. From the figure it is interesting to note that although the reference distributions for the top and the bottom walls are initially different, after optimization they are almost identical. The trend is to increase the thicknesses at the root and then significantly reduce the thickness with near linear taper up to approximately 75 percent span. Near the tip, the thicknesses are slightly above the value at 75 percent span location but are still drastically reduced from the reference values (28.5 and 22.5 percent, respectively for the top and bottom walls). This is explained as follows. Near the root, the thicknesses are increased to satisfy the stress constraints which are initially violated. Since only the root stresses are critical in this formulation, the optimizer is now able to reduce the distributions throughout the span in order to reduce the wing weight. To ensure that the aeroelastic stability constraints are not violated (Fig. 11), the thicknesses near the tip are held nearly constant (relative to the 75 percent span value). The very small increases in the tip values, from the 75 percent span location, are due to the nature of the orthogonal functions used in the formulation of the thickness distributions. If more higher order orthogonal functions were included in the formulation, the tip values would very likely equal the values at 75 percent span. It must be noted that the cause of the initial constraint violation of the reference wing is due to the assumption of the box beam model. In order to closely match the natural frequencies,

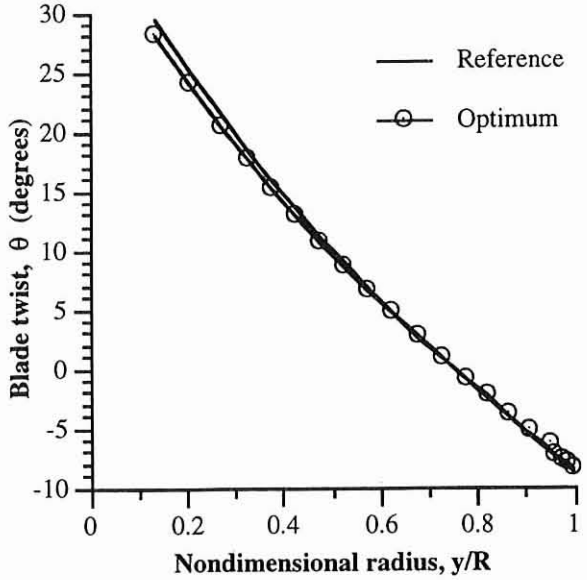

Fig. 8. Blade twist distributions.

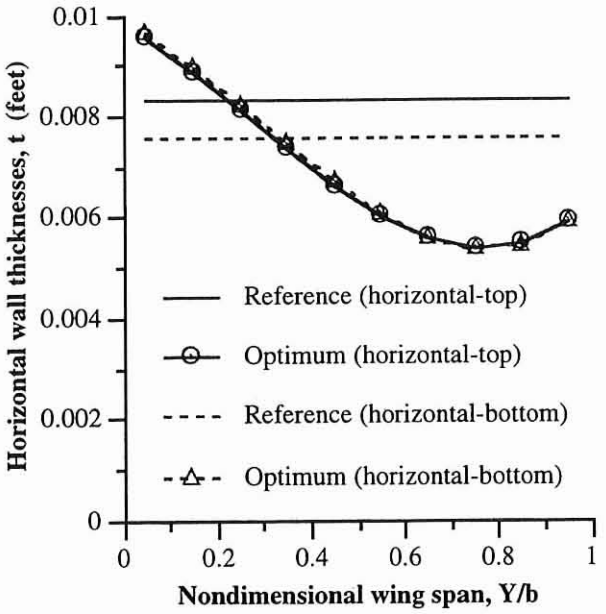

Fig. 10a. Horizontal wall thicknesses distributions.

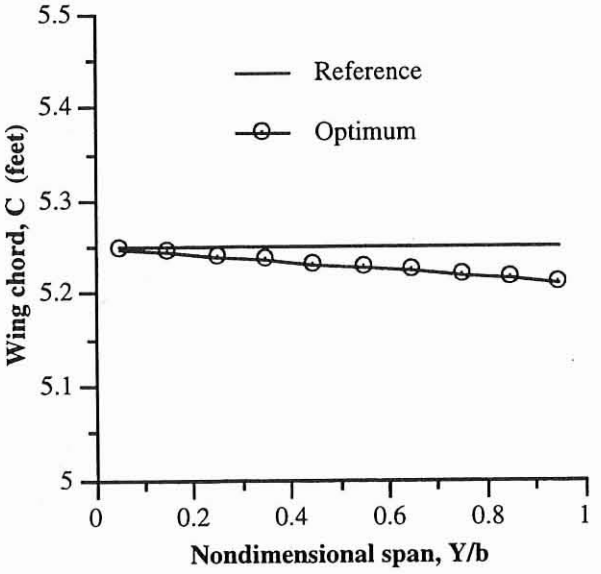

Fig. 9. Wing chord distributions.

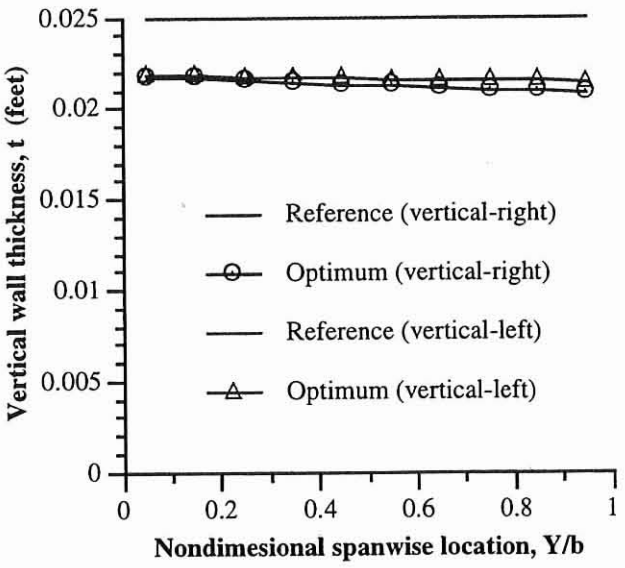

Fig. 10b. Vertical wall thicknesses distributions.

generalized masses and generalized mode shapes of the actual structural assembly which consists of stringers, spars and webs, the thickness distribution of the rectangular box beam produces stress constraints which are slightly violated initially. A more accurate representation of the wing structural elements is necessary for detailed studies in rotary wing performance.

The vertical wall thickness distributions are presented in Fig. 10b and shows that the optimum distributions are reduced from reference values throughout the blade span, including at the root. It must be noted here that the reference distributions in this case are the same for both the right and the left walls. The increased stiffnesses required to satisfy the stress constraints were achieved through an increase in the root thickness of the horizontal walls. Therefore, the optimizer is able to reduce the vertical wall thicknesses throughout the blade span to reduce the wing weight. It is of interest to note that despite the fact that cubic distributions are assumed for the vertical wall thicknesses, the optimum distributions in both cases essentially have only slight linear taper.

The first three mode shapes for the wing are presented in Figs. 12-14. The first mode (Fig. 12) is primarily an out-of-plane (flapping) motion. The second mode (Fig. 13) represents an inplane (chordwise bending) dominated motion and the third mode (Fig. 14) is a pitching (elastic twist) dominated motion. The figures also show the primary coupling associated with each mode. In Fig. 12 it is seen that the flapping motion of the first mode is slightly reduced from reference to optimum configuration. The coupling due to the pitching, however, is actually slightly increased in this mode. From Fig. 13 it is seen that the modes shapes for the second mode, which is primarily a lagging mode, are virtually unchanged after optimization. The third mode, which represents a pitching dominated mode, is presented in Fig. 14 where

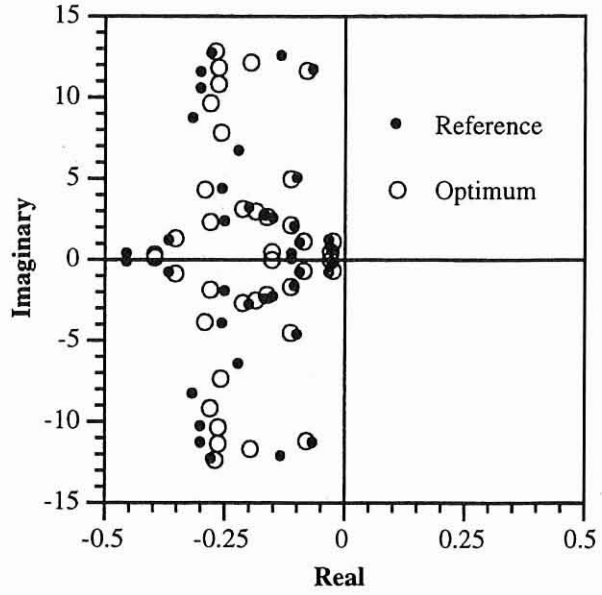

Fig. 11. Aeroelastic stability characteristic exponents.

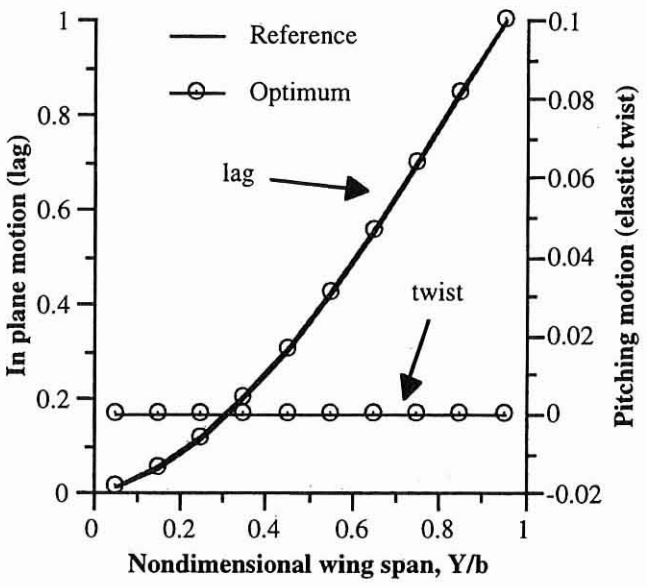

Fig. 13. Second wing mode.

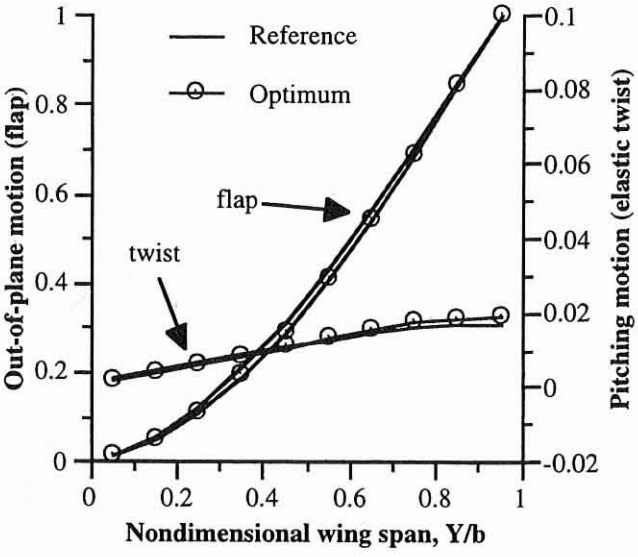

Fig. 12. First wing mode.

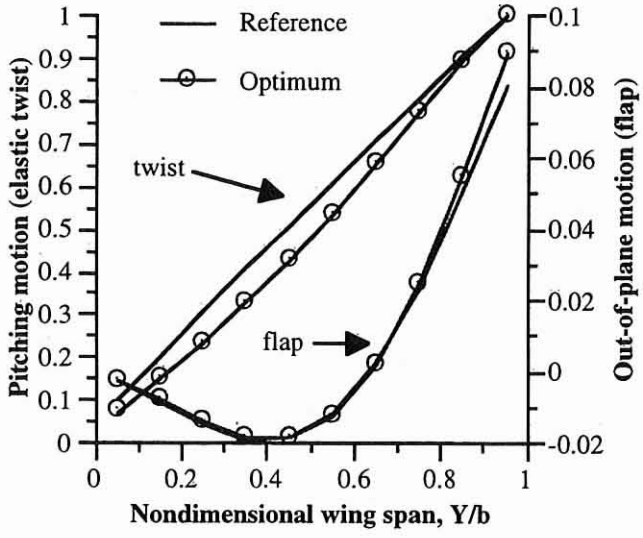

Fig. 14. Third wing mode.

once again it is seen that primary mode is slightly reduced from reference to optimum, but the coupling, which in this case is due to the flapping motion, is again increased. The slight increases in the coupling of the wing modes are explained as follows. Wing weight minimization, one of the objectives, is accomplished through reductions of the wall thicknesses in the wing box beam and through the introduction of a slight wing chord taper. This results in small decreases in the wing stiffnesses and therefore small increases in the coupling of the mode shapes. A significant reduction in stiffnesses can increase whirl flutter instabilities. However, as shown in Fig. 11, although the aeroelastic stability constraints are made slightly more critical after optimization, they still remain stable. This is an important phenomenon and points to the critical trade-offs associated with optimum design for minimum wing weight while maintaining aeroelastic stability.

It must be noted that although the results presented in this paper do provide qualitative insight into the optimization of a coupled rotor/wing system, a more comprehensive wing analysis is necessary to provide detailed design information. Also in CAMRAD there is no aerodynamic feedback from the wing to the rotor. Therefore using this modeling technique, only the influence of the rotor on the wing can be investigated. For future work it is recommended that a lifting panel code be used to calculate the aerodynamic loads for the both the rotor and the wing. This aerodynamic algorithm could then be coupled with a comprehensive finite element model to accurately calculate the complete equations of motion for the coupled rotor/wing configuration.

Concluding Remarks

A multidisciplinary optimization procedure is developed to analyze the coupled rotor/wing design for proprotor aircraft. The optimization

procedure couples aerodynamic performance, aeroelastic stability and structural design for both high speed cruise and hover flight conditions. Objective functions include the simultaneous maximization of the hover figure of merit and the high speed cruise propulsive efficiency and the minimization of the wing weight. Constraints are imposed on the first natural frequency in hover, the autorotational inertia, the blade weight and the maximum wing root stresses. To prevent whirl flutter, constraints are also imposed on the real part of the stability roots. In addition, geometric constraints are also imposed. The optimization procedure is performed using the Kreisselmeier-Steinhauser (K-S) function technique and the Broyden-Fletcher-Goldfarb-Shanno (BFGS) algorithm. To reduce computational effort, an approximate analysis procedure based on the two-point exponential expansion and variable move limits is used. The results obtained are compared with an existing reference tilt-rotor configuration. The following important observations are made from this study.

1. Significant improvements are obtained in hover figure of merit and wing weight with small improvements in high speed cruise propulsive efficiency. The combined rotor/wing weight is also reduced significantly.
2. The blade chord distribution is increased over the midspan region to exploit portions of the blade which simultaneously improve both the hover and high speed cruise performance. The chord distribution near the root and the tip are reduced due to the conflicting requirements posed by hover and cruise conditions.
3. Wing weight reductions are achieved through reductions in the wall thicknesses although the horizontal walls are increased at the root to satisfy the root stress constraints which are violated in the reference design. The wing chord is only slightly tapered to maintain aeroelastic stability requirements.
4. Reduction in wing weight results in small reductions in stiffness in the optimum configuration. This leads to increased coupling in wing modes. However, stability is still maintained in the optimum configuration.

Acknowledgments

The authors would like to acknowledge support of this work through grants from the NASA Ames Research Center, Grant numbers NAG2-771 and NCC2-795, technical monitor Dr. Sesi Kottapalli. The authors also appreciate the valuable technical assistance offered by Mr. John F. Madden, III of the Ames Research Center.

References

[1]Felker, F. F., "Wing Download Results from a Test of a 0.658-Scale V-22 Rotor and Wing," *Journal of the American Helicopter Society,* Vol. 37, No. 4, Oct 1992, pp. 58-63.

[2]Chattopadhyay, A. and Narayan, J., "Optimum Design of High Speed Prop-Rotors Using a Multidisciplinary Approach," *Engineering Optimization,* Vol. 22, pp. 1-17, 1993. Also presented at the 48th Annual Forum of the American Helicopter Society, June 3-5, 1992, Washington, DC.

[3]McCarthy, T. R. and Chattopadhyay, A, "Design of High Speed Proprotors Using Multiobjective Optimization Techniques," *Engineering Optimization* (in press).

[4]Chattopadhyay, A., McCarthy, T. R. and Madden, J. F., "Structural Optimization of High Speed Prop Rotors Including Aeroelastic Stability Constraints," *Mathematical and Computer Modelling,* Special Issue on Rotorcraft, Vol. 18, No. 3/4, pp. 101-113, 1993.

[5]Chattopadhyay, A., McCarthy, T. R. and Madden, J. F., "A Design Optimization Procedure for Minimizing Drive System Weight of High Speed Prop-Rotors," *Engineering Optimization,* Vol. 23, No. 4 (in press). Also presented at the 4th AHS Rotorcraft Specialists Meeting on Multidisciplinary Design Optimization, Atlanta, Georgia, Apr 1993.

[6]Chattopadhyay, A., McCarthy, T. R. and Madden, J. F., "An Optimization Procedure for the Design of Prop Rotors In High Speed Cruise Including the Coupling of Performance, Aeroelastic Stability and Structures" *Mathematical and Computer Modelling,* Special Issue on Rotorcraft, Vol. 19, No. 3/4, pp. 75-88, 1994. Also presented at the 49th Annual AHS Forum, St. Louis, Missouri, June 1993.

[7]McCarthy, T. R., Chattopadhyay, A., Talbot, P. D., and Madden, J. F., "A Performance Based Optimization of High Speed Prop-Rotors," *Journal of the AHS* (in press). Also *Proc.* of the American Helicopter Society Aeromechanics Specialists Conference, San Francisco, Jan 1994.

[8]Chattopadhyay, A., McCarthy, T. R. and Seeley, C. E., "A Decomposition Based Optimization Procedure for High Speed Prop-Rotors using Composite Tailoring and Simulated Annealing," *Proc.* 50th Annual AHS Forum, Washington, DC, May 1994. Also submitted to *Journal of Aircraft,* June 1994.

[9]Acree, C. W. and Tischler, M. B., "Identification of XV-15 Aeroelastic Modes Using Frequency Sweeps," *Journal of Aircraft,* Vol. 26, No. 7, pp. 667-674, July 1989.

[10]Lamon, S., "XV-15 Advanced Technology Blades, Ultimate Stress Analysis," Boeing Report Number D210-12345-1, 1985.

[11]Chattopadhyay, A. and McCarthy, T. R.., "Multiobjective Design Optimization of Helicopter Rotor Blades with Multidisciplinary Couplings," *Optimization of Structural Systems and Industrial Applications,* editors, Hernandez, S. and Brebbia, C.A., pp. 451-462, 1991.

[12]Johnson, W, "A Comprehensive Analytical Model of Rotorcraft Aerodynamics and Dynamics, Part II: User's Manual," NASA TM 81183, June 1980.

[13]Nixon, M. W., *Aeroelastic Response and Stability of Tiltrotors with Elastically-Coupled Composite Rotor Blades,* Ph. D. Dissertation, Department of Aerospace Engineering, University of Maryland, College Park, Maryland 1993.

[14]Kreisselmeier, A. and Steinhauser, R., "Systematic Control Design by Optimizing a Vector Performance Index," *Proc.* of IFAC Symposium on Computer Aided Design of Control Systems, Zurich, Switzerland, 1979, pp. 113-117.

[15]McCarthy, T. R., Chattopadhyay, A., Talbot, P. D. and Madden, J. F., III, "A Performance Based Optimization of High Speed Prop-Rotors," *Journal of the American Helicopter Society,* Vol. 40, No. 3, July 1995, pp. 92 - 100.

[16]Fadel, G. M., Riley, M. F. and Barthelemy, J. M., "Two Point Exponential Approximation Method for Structural Optimization," *Structural Optimization,* Vol. 2, pp. 117-224.

[17]Haftka, R. T., Gürdal, Z. and Kamat, M. P., *Elements of Structural Optimization,* Kluwer Academic Publishers, Dordrecht, The Netherlands, 1990.

[18]Thomas, H. L., Vanderplaats, G. N., Shyy, Y-K, "A Study of Move Limit Adjustment Strategies in the Approximation Concepts Approach to Structural Synthesis," *Proc.* 4th AIAA/USAF/NASA/OAI Symposium on Multidisciplinary Analysis and Optimizations, Cleveland, OH, Sept 1992. AIAA Paper No. 92-4750-CP.